ISSN 1063-7826, Semiconductors, 2014, Vol. 48, No. 9, pp. 1178–1184. © Pleiades Publishing, Ltd., 2014.
Original Russian Text © V.G. Talalaev, G.E. Cirlin, L.I. Goray, B.V. Novikov, M.E. Labzovskaya, J.W. Tomm, P. Werner, B. Fuhrmann, J. Schilling, P.N. Racec, 2014, published in Fizika i Tekhnika Poluprovodnikov, 2014, Vol. 48, No. 9, pp. 1209–1216.

SEMICONDUCTOR STRUCTURES, LOW-DIMENSIONAL SYSTEMS, AND QUANTUM PHENOMENA

Effect of Nanobridges on the Emission Spectra of a Quantum Dot–Quantum Well Tunneling Pair

V. G. Talalaev[a,b,c,d^], G. E. Cirlin[d,e,f,g,j], L. I. Goray[e,g], B. V. Novikov[d], M. E. Labzovskaya[d], J. W. Tomm[c], P. Werner[a], B. Fuhrmann[h], J. Schilling[b,h], and P. N. Racec[i]

[a] *Max Planck Institute of Microstructure Physics, 06120 Halle (Saale), Germany*

[^] *e-mail: talalaev@mpi-halle.mpg.de*

[b] *Martin Luther University Halle-Wittenberg, ZIK SiLi-nano, 06120 Halle, Germany*

[c] *Max Born Institute for Nonlinear Optics and Short Pulse Spectroscopy, 12489 Berlin, Germany*

[d] *Fock Institute of Physics, St. Petersburg State University, ul. Ul'yanovskaya 1, Petrodvorets, St. Petersburg, 198504 Russia*

[e] *Saint Petersburg Academic University–Nanotechnology Research and Education Center, Russian Academy of Sciences, ul. Khlopina 8/3, St. Petersburg, 194021 Russia*

[f] *Ioffe Physical–Technical Institute, Russian Academy of Sciences, ul. Politekhnicheskaya 26, St. Petersburg, 194021 Russia*

[g] *Institute for Analytical Instrumentation, Russian Academy of Sciences, Rizhsky pr. 26, St. Petersburg, 190103 Russia*

[h] *Martin Luther University, Interdisciplinary Center of Materials Science, 06120 Halle, Germany*

[i] *Weierstrass Institute for Applied Analysis and Stochastics, 10117 Berlin, Germany*

[j] *Saint Petersburg State Polytechnic University, ul. Politekhnicheskaya 29, St. Petersburg, 195251 Russi*

Submitted December 25, 2013; accepted for publication January 24, 2014

Abstract—Emission in the narrow spectral range 950–1000 nm is obtained at the nanobridge optical transition involving experimentally and theoretically observed hybrid states in the InGaAs system, i.e., quantum dot–nanobridge–quantum well. It is experimentally shown that the oscillator strength of the new transition sharply increases in the built-in electric field of a *pin* junction. In the mode of weak currents in the system under study, the nanobridge transition is the dominant electroluminescence channel. At current densities >10 A cm^2, nanobridge "burning" is observed, after which the system becomes a "quasi-classical" quantum dot–quantum well tunneling pair separated by a barrier.

DOI: 10.1134/S1063782614090218

1. INTRODUCTION

Recently, nanostructures with tunnel-coupled components, from a separate class of quantum-well heterostructures, have become more and more common model objects of fundamental research. Simultaneously, new prospects have been uncovered for the practical applications of tunnel-coupled systems. Heterostructures with nanocomponents of the same dimensionality (two-dimensional such as quantum well–quantum well or zero-dimensional such as quantum dot–quantum dot), but with different potential-well depths are known as tunnel-injection structures (TISs). The combination of elements with different dimensionality in a single system, e.g., a tunneling pair consisting of a quantum well (QW) and a quantum dot (QD), introduces new "intrigue" in this direction, since this requires a new fundamental approach and reveals new prospects for modern nanophotonics. Theoretically proposed heterolasers based on QW–QD TISs [1] were almost simultaneously implemented in practice [2, 3] with a threshold current of 180 A cm^{-2} [4]. The new emitter was called a tunnel-injection QD laser and contained a "direct" sequence of layers in the growth direction, i.e., QW–barrier–QD. The spatial separation of the injector (QW) and nanoemitter (QD) provides a new degree of freedom in designing the laser active region, i.e., the possibility of "fitting" the QW and QD energy spectra. Due to the tunneling of "cold" carriers from the QW to the QD ground state, internal losses, diffusion capacitance, and threshold current are significantly decreased, and the operating speed and differential efficiency of laser diodes increase.

As previously reported [5–8], we changed the direct sequence of layers in the QW–QD TIS to the inverse variant: InGaAs QD–GaAs barrier–InGaAs QD. Inversion of the nanolayers retains all the advantages of the conventional TIS. The QW due to the large trapping cross section and capacitance as before plays the role of an efficient injector of carriers into the QD which has high thermal stability of emission and operates as a light emitter. The existence of the tunnel barrier between the QW and QD provides an additional degree of freedom and the injection of "cold" carriers, which immediately populate the QD ground state. Furthermore, nanolayer inversion in the TIS led to an entirely new result, i.e., the appearance of a quasi-

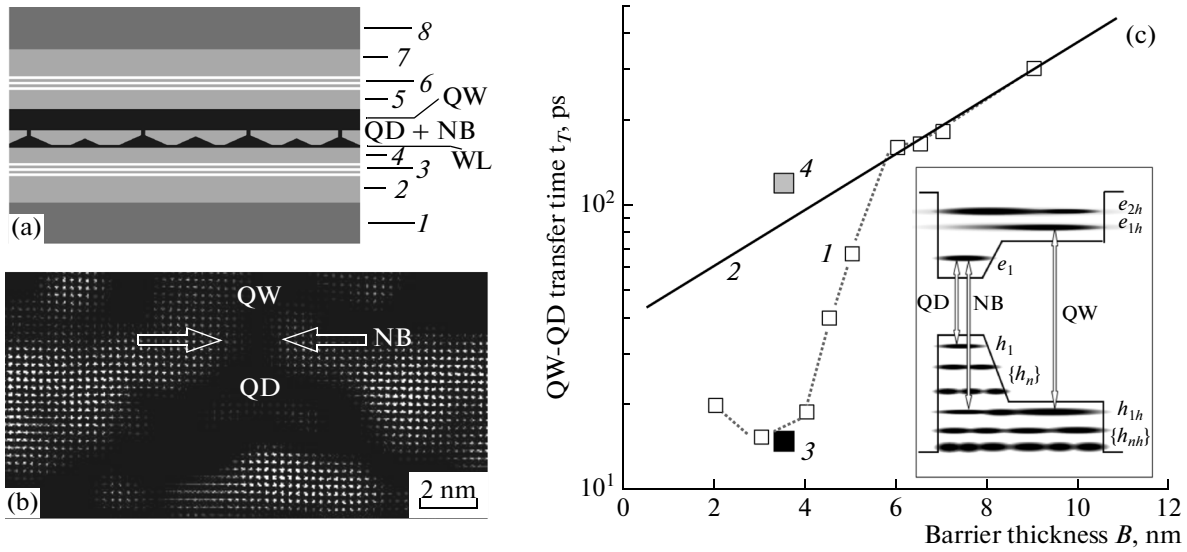

Fig. 1. (a) Scheme of the layer sequence in the *i*-TIS (see text for details). (b) High-resolution TEM image of the tunneling pair consisting of a QD and QW and a nanobridge (NB). (c) Time of excitation transfer from QW to QD (τ_T) as a function of the barrier thickness *B*: (*1*) QD–QW *i*-TIS, (*2*) WKB approximation, (*3*) *i*-TIS with a barrier $B = 3.5$ nm before nanobridge burning, (*4*) the same *i*-TIS after nanobridge burning; the values of τ_T were obtained by analyzing the QD PL kinetics; the inset shows the energy-level diagram and ground-state transitions in the *i*-TIS.

point contact (nanobridge) between the QD top and QW bottom, separated by a thin barrier. The nanobridge (NB) results in the disappearance of this barrier and "immediate" carrier injection from the QW to the QD. Thus, the restrictions on the carrier flux density associated with its tunneling exponential depletion are removed.

In this work, we continue the study of inverted QD–QW TISs (*i*-TISs) with InGaAs nanobridges. The main manifestations of nanobridges in the *i*-TIS emission spectra (NB band) are determined. An increase in the oscillator strength of the NB radiative transition is detected in the built-in field of the *p–n* junction and(or) under conditions of current flow through the QD–NB–QW structure. The electroluminescence is studied and current conditions of nanobridge operation are determined. The theoretical *i*-TIS model based on the concept of state hybridization in the InGaAs QD–NB–QW system is developed and justified.

2. SAMPLES AND EXPERIMENTAL

Experimental InGaAs/GaAs *i*-TISs with QD–QW tunneling pairs built in *pin* (or *nip*) junctions were grown by molecular-beam epitaxy. As substrates, *p*-type (or *n*-type) GaAs (100) wafers were used. The layer sequence in the samples is shown in Fig. 1a. After depositing a buffer layer (*1*) 300 nm thick doped with Be (or Si) to a concentration of 5×10^{18} cm^{-3} to attain *p*-type (or *n*-type) conductivity and an undoped GaAs layer (*2*) 20 nm thick, an $Al_{0.25}Ga_{0.75}As$/GaAs superlattice (2.5 nm/2.5 nm) × 3 (*3*) and a waveguide layer of undoped GaAs (*4*) 20 nm thick were grown. Then the substrate temperature was lowered from 550 to 485°C and an active region was grown by the sequential deposition of two InAs monolayers from which a QD, a GaAs spacer 3.5 nm thick, and an $In_{0.15}Ga_{0.85}As$ QW 10 nm thick were formed by the Stranski-Krastanov mechanism. At the final growth stage, the substrate temperature was increased to 550°C and a layer sequence similar to (*1–4*), but in reverse order (*5–8*), with dopant replacement in the upper layer (*8*).

Discrete light emitters were fabricated from the grown nanostructures. A mesa structure 1.4 mm in diameter was formed by photolithography and reactive jet ion–plasma etching. Its base was a *p*-type buffer layer. Ohmic contacts were deposited by vacuum thermal evaporation and were shaped by photolithography as plane rings. The lower ring to the *p*-type layer (with an outer diameter of 2.2 mm) was made of gold–zinc eutectic; the upper ring to the *n*-type layer was made of gold-germanium eutectics. The inner diameter of this ring (0.8 mm) formed the output window of the light emitter. Both eutectic layers were strengthened by gold 100 nm thick, after which contacts were annealed at a temperature of 250°C. The chip with a mesa structure was soldered with gold wire in a TO-39 socket. The mesa-structure geometry and contact ohmicity were retained when fabricating light emitters based on the QD–QW tunneling pair built in the *nip* junction.

The structural properties of the samples were studied by transmission electron microscopy (TEM) including high-resolution TEM (Fig. 1b). According to the TEM data, $In_{0.6}Ga_{0.4}As$ QDs lie on a thin wetting layer (WL) of the same composition, and the array density is 5×10^{10} cm^{-2}.

The photo- and electroluminescence spectra were measured in the synchronous detection mode using a cooled germanium photodetector interfaced with a 0.5-meter ARC monochromator. The photoluminescence (PL) was excited by the 488-nm (2.54 eV) line of an argon laser; the electroluminescence (EL) was excited by a Thorlabs pulsed current generator for laser diodes. The study was performed in optical cryostats at a temperature of 10 K. The excitation spectra were measured using a Koheras continuous-spectrum laser source. A spectral width of 5 nm was excited by an ARC monochromator. The PL kinetics was studied upon excitation by a Spectra Physics laser (wavelength is 785 nm, frequency is 82 MHz, and pulse duration is 100 fs) using a Hamamatsu streak camera with a time resolution of 5 ps.

The PL excitation density in the *pin* (or *nip*) junction, produced by the *i*-TIS, was far from values which result in compensation for the built-in potential difference by photovoltage. The pump density was 5 W cm^{-2} for steady-state PL, 0.5 W cm^{-2} for the PL excitation spectra, and 5×10^{11} photon cm^{-2} per pulse for the time-resolved PL spectra. The second harmonic of a Light Conversion pulsed laser (515 nm, 1 kHz, 200 fs) was specially used to study the effect of the PL excitation power. The maximum excitation density per pulse not leading to sample heating was 10^{17} photon cm^{-2}.

3. MODEL, RESULTS, AND DISCUSSION

It is not difficult to imagine the model of an ideal tunnel-coupled QW–WD pair in which the following requirements are fulfilled: the injector ground level (QW) is between the emitter ground and first excited levels (QD), and a high rate of "cold" carrier transfer from the injector level to the emitter ground level is provided.

The first requirement causes no difficulties and can be fulfilled by selecting the indium concentration and InGaAs QW and QD sizes. The implementation of this requirement for the electronic subsystem was presented previously for the QD–QW *i*-TIS [5–8]. For the hole subsystem with higher densities of states in the QW and QD potential wells, fulfillment of this requirement is not so obvious.

The second component of the QW–QD model is associated with tunneling whose features are currently studied for equidimensional elements (QW–QW [9–11] and QD–QD [12–14]). However, tunneling transport in structures with combined dimensionality such as QW–QD began to be studied relatively recently [5, 15]. To date, independent results have been obtained, on the basis of which it is concluded that the carrier-tunneling rate in tunnel-injection InGaAs nanostructures with a "direct" sequence of QW–QD layers, at GaAs barrier thicknesses from 2 to 20 nm, is described by the quasi-classical Wentzel–Kramers–Brillouin (WKB) approximation, i.e., by an exponential dependence [7, 16]. If the exponential limit of the tunneling rate is retained at any barrier thickness, this can cancel out efforts to achieve a high emission efficiency in the QW–QD TIS. The above threshold current density in tunnel-injection QD lasers (180 A cm^{-2}) has not yet been lowered and is still far from record values [4].

We previously proposed an approach which is beyond the quasi-classical WKB approach and overcomes the exponential limit of the rate of carrier tunneling from QW to QD [5]. We deal for the first time with the "inverted" layer sequence in the TIS: (lower $In_{0.6}Ga_{0.4}As$ QD layer)–(GaAs barrier)–(upper $In_{0.15}Ga_{0.85}As$ QW layer). For such *i*-TISs, deviations from the WKB model, i.e., a reduction in transport time to several picoseconds, were detected (Fig. 1c). The high-resolution TEM data showed that point contacts between the QD tops and the QW layer, i.e., nanobridges, were formed in the *i*-TIS (Fig. 1b).

This phenomenon is based on elastic strains which form an indium-enriched channel 2 nm in section upon overgrowth of the QD top with a GaAs spacer layer. QD and QW coupling through InGaAs nanobridges was observed to spacer thicknesses of $B =$ 6 nm. Due to the variable indium content in the nanobridge ($0.15 \le x \le 0.6$), the barrier between the QW and QD disappears, and a uniform quantum-confinement region is formed. As a result, the nanobridge becomes an element coupling the QW and QD states into a single hybrid system of levels (see the inset in Fig. 1c). This provides almost immediate carrier transfer from the injector (QW) through nanobridges to the light emitter (QD), which results in an increase in the emission efficiency by an order of magnitude.

Figure 1c shows that the carrier transfer time τ_T in a QD–NB–QW *i*-TIS based on InGaAs at a barrier thickness of $B < 6$ nm is sharply reduced, deviates from the exponential dependence (WKB approximation) and is limited only by the instrumental resolution and the inhomogeneity of the barrier thickness. A more accurate approach based on $\tau_T(B)$ measurements for several TIS series shows that the region of deviation from the WKB approximation is also limited from below. We can see in Fig. 1c that the quasi-classical dependence is restored at $B < 2$ nm, i.e., the effect of nanobridges disappears.

To correct the physical model, with which we deal in the case of *i*-TIS with nanobridges, in what follows, we present the main conclusions following from solution of the three-dimensional Schrödinger equation by the volume element method with Dirichlet boundary conditions in the cylindrical coordinate system [17].

Calculations were performed to determine the energy spectrum, wavefunctions, and matrix elements of junctions in the system of an $In_{0.6}Ga_{0.4}As$ QD and an $In_{0.15}Ga_{0.85}As$ QW coupled by a 2-nm-diameter InGaAs nanobridge from 1 to 10 nm long of variable composition with an indium content from 0.15 to 0.6. It was shown that the perturbation introduced by the nanobridge has an effect predominantly on the hole

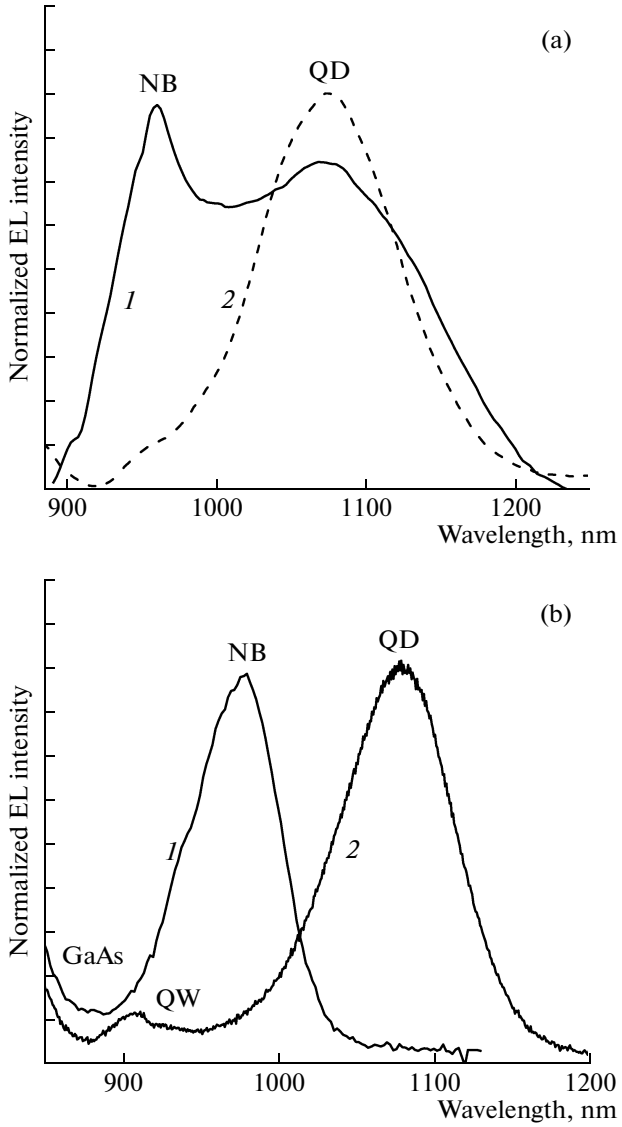

Fig. 2. Photoluminescence (PL) and electroluminescence (EL) spectra of the *i*-TISs with the same barrier thickness $B = 3.5$ nm. (a) PL: (*1*) *i*-TIS in the *pin* junction, (*2*) *i*-TIS in the *nip* junction. (b) EL for various current densities J: (*1*) low-current mode, $J = 3$ A cm^{-2} (before nanobridge burning); (*2*) nanobridge burning mode, $J = 20$ A cm^{-2}.

subsystem. It also follows from the calculations that a single nanobridge >1.5 nm long has hole eigenstates.

For the complete QD–NB–QW system, this result remains valid. Depending on the quantum number, the hole wavefunction is distributed along the system axis with variable density, having regular antinodes no less than 2 nm long within the nanobridges. A comparison of this result with the experimental dependence in Fig. 1c leads to the conclusion that the new hybrid hole state h_{1h} plays the role of a "trigger" for deviation of the dependence $\tau_T(B)$ from that described by the WKB approximation and enhancement of the carrier exchange between the QW and QD.

In contrast to holes, the electronic subsystem weakly responds to the nanobridge appearance. If we consider the wavefunctions of final states, transitions between which could appear in the optical spectra of the QD–NB–QW system, it turns out that such electron and hole wavefunctions are localized in the QDs (state e_1) and QWs (state h_{1h}).Calculation of the matrix elements of optical transitions showed that the oscillator strength of the ground transition e_1–h_{1h} is too small (probability density is <0.1) due to the above features of the localization of electron and hole wavefunctions of the QD–NB–QW system. For higher states and a small NB length (B = 2–6 nm), the hybridization effects are very strong, and the oscillator strength of the transitions drastically changes, passing through a maximum in the range B = 4–5 nm. It is clear that experimental observation of the e_1–h_{1h} transition requires a shift of the hole wavefunction to the QD region.

Wavefunction redistribution is possible, e.g., in an electric field and(or) under conditions of current flow through the structure. Since the goal of the present study is the implementation of a TIS-based emitter, this requirement is naturally fulfilled when developing the *p*–*n* junction. In this regard, we analyzed the experimental data relating to the luminescence of the TIS with an inverted layer sequence (*i*-TIS) embedded in the intrinsic region of the *pin* structure and having a barrier layer <6 nm thick between the QD and QW.

The PL excitation spectrum of the *i*-TIS with a barrier of $B = 4.5$ nm in the *pin* junction, we presented previously in comparison with the spectra of the *i*-TIS without a built-in electric field [18], proves that the NB band at a wavelength of 960 nm (1.3 eV) is a new one inherent to only this structure and, hence, can be attributed to the e_1–h_{1h} transition involving a new hybrid hole state with a shifted wavefunction in the QD–NB–QW system. The NB band for the *i*-TIS with a thin barrier in the *pin* junction was also recorded in PL spectra, whereas similar structures embedded in the *nip* junction contained no distinct NB band. We illustrate this feature in Fig. 2a using the PL spectra of the *i*-TIS with a barrier thickness (nanobridge length) of 3.5 nm.

The NB radiative transition between the electron ground state e_1 in the QD and one of the hybrid hole states (e.g., h_{1h}) of the complete QD–NB–QW system becomes experimentally detectable provided the following conditions are satisfied: (i) the e_1–h_{1h} transition is allowed by the selection rules (magnetic indices are identical); (ii) the squares of the wavefunctions $|\Psi_{e_1}|^2$ and $|\Psi_{h_{1h}}|^2$ overlap; (iii) the relaxation of holes from the hybrid h_{1h} level to low-energy QD states is not too fast in comparison with the emission time in the NB band. Since the first condition is easily satisfied for a set of closely packed hole levels, we pass to the second condition. The density of the QD e_1 electronic state not subjected to hybridization effects is concen-

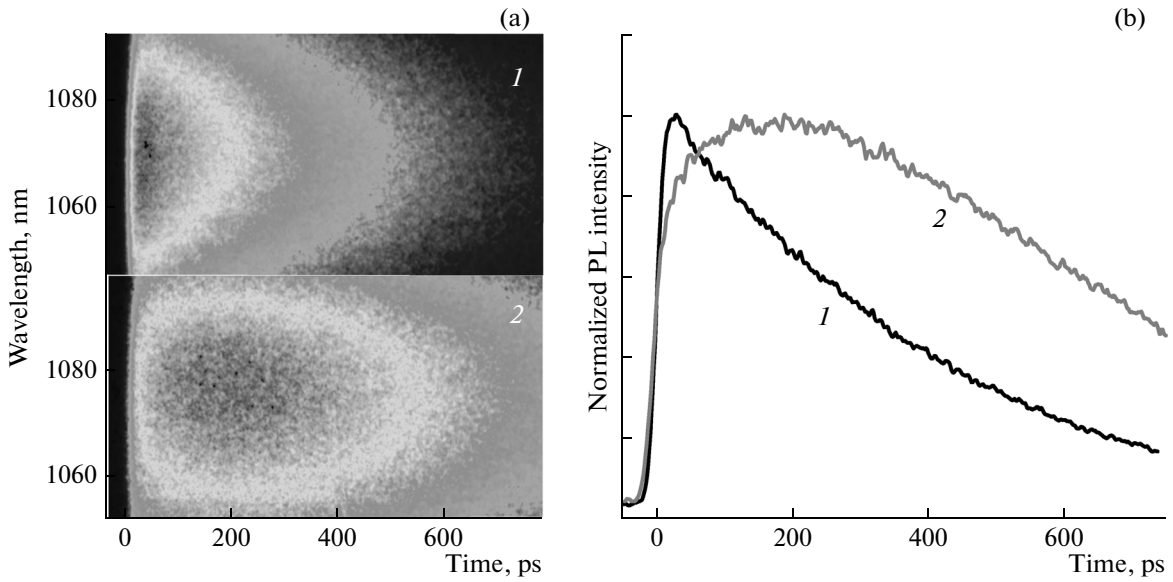

Fig. 3. PL kinetics of the QD for the *i*-TIS with barrier thickness $B = 3.5$ nm. (a) Original screenshots from the streak camera, (b) PL time profiles (*1*) before and (*2*) after nanobridge burning.

trated in the QD itself. The hole wavefunction of the hybrid state h_{1h} can be shifted to the QD region by the built-in electric field of the *pin* junction. On the contrary, the *nip* junction self-field "presses" the hole wavefunction of the system to the QW.

Thus, the new e_1–h_{1h} transition gains oscillator strength and becomes observable only in experiments with *pin* structures.

The new NB band becomes dominant in the EL spectra in the case of low currents through the *i*-TIS (to 5 A cm^{-2}), and the QD signal disappears (Fig. 2b). In the mode of low currents, the total intensity A of the NB band increases with current density J according to the law $A \propto J^K$, which is close to linear ($0.8 \le K \le 1.3$ depending on the *i*-TIS). At a current density of $J >$ 5 A cm^{-2}, the NB intensity flattens and, near 10 A cm^{-2}, abruptly decreases. At a current density of $J > 10$ A cm^{-2}, another EL phase begins: the NB band almost disappears from the spectrum; however, the QD emission band appears (Fig. 2b), whose intensity increases according to superlinear law ($(5 \le K \le 12)$ depending on the structure). In some cases, the mode of "strong" currents led to lasing at the long-wavelength slope of the QD band. In this case, the threshold current density in the *i*-TIS at low temperatures was ten times lower than the known values for tunnel-injection QD lasers with a direct layer sequence [4].

Such an extraordinary current dependence of the EL spectrum of the *i*-TIS becomes explainable within the same QD–NB–QW model. If we suppose that half the QD arrays contain 2-nm-diameter nanobridges coupling them with QWs, and other current leakage paths are lacking, the current density through the nanobridges will be no less than 10 kA cm^{-2} at the average value $J = 10$ A cm^{-2} for the total mesa-structure section. This value seems sufficient for InGaAs nanobridge "burning". Insulating nanoplugs are formed at their sites, which represent high potential barriers in the energy diagram. The system of hybrid levels is destroyed, a QD fraction is removed from the carrier-transport process, and the electric current flows through the remaining QDs having no nanobridges. This probably explains the low average threshold currents for lasing in the *i*-TIS. Thus, nanobridge "burning" allows an efficient decrease in the average lasing threshold in such structures.

Nanobridge burning should reduce the carrier injection rate from the QWs to QDs. To test this model, we determined the carrier transport times between QWs and QDs in the mesa structure with the *i*-TIS ($B = 3.5$ nm) before and after passing an electric current with an average density of >10 A cm^{-2} through it. The indicator of nanobridge burning was the appearance of the EL signal from the QDs (the QD band in Fig. 2b). The measurements were performed using the same technique and under the same conditions we used previously (see Fig. 1c) and are described in [5, 6]. The original streak camera screenshots and the PL kinetics in the QD band are shown in Fig. 3. In this case, the time of carrier transfer from QW to QD was determined from the QD PL growth kinetics in the QD band. As before [5, 6], this time correlated well with the PL decay time in the QW band. Thus, the time of transfer from QW to QD (τ_T) after nanobridge burning increased from 15 to 120 ps, i.e., almost returned to the "quasi-classical" tunneling time in the absence of nanobridges (Fig. 1c).

At a high spectral resolution, we succeeded in recording the fine structure of the NB PL band (Fig. 4a) which reflects the contribution of the high-

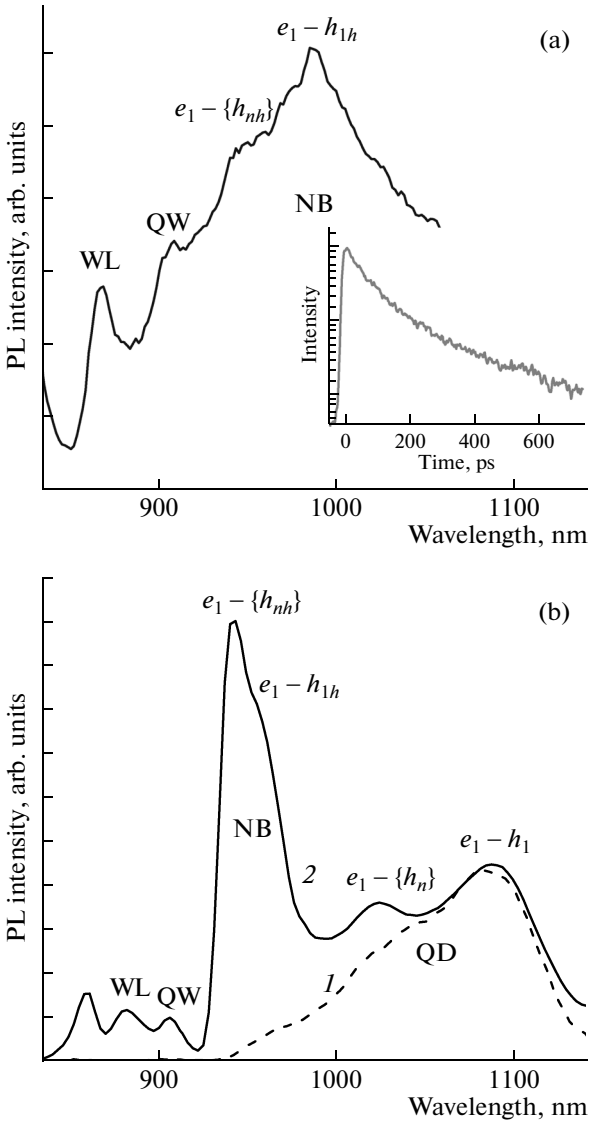

Fig. 4. PL spectra of the *i*-TIS with the same barrier thickness $B = 3.5$ nm. (a) NB band detailing upon steady-state excitation; the inset shows the time profile of the NB band. (b) The pulsed excitation power is (*1*) 2×10^{13} and (*2*) 10^{17} photon cm^{-2}; the spectra are normalized to the intensity of the e_1–h_1 transition of the QD PL band.

energy hybrid states $\{h_{nh}\}$ of the QD–NB–QW hole subsystem. The PL kinetics of the main NB band is shown in the inset of Fig. 4a. The NB PL decay is described by two exponents with characteristic times of 100 and 700 ps. The long-term component reflects the exciton emission time in the QD–NB–QW system, which appears very close to the e_1–h_1 exciton radiative lifetime in a QD (750 ps) [5, 6].

The first short-time component of the NB PL decay (100 ps) is associated with the hole relaxation of excitation from the hybrid h_{1h} state to low-energy QD states $\{h_n\}$ and corresponds to the dependence of the relaxation time of excitons on the barrier thickness, we previously obtained in [8]. Thus, the frameworks for satisfying the third condition for strengthening the NB transition are defined. In contrast to lighter electrons, holes from the hybrid levels relax in QDs through numerous intermediate states $\{h_n\}$ rather slowly to make the NB junction significant in the steady-state emission spectra of the *i*-TIS. The likely explanation of slow hole relaxation is the effect of filling the lowest hole states of the QDs during direct photon absorption. The stable enough number of photogenerated holes in the QD ground state h_1 leads to that the final PL-increase kinetics in the QD band, hence, the rate of excitation transfer from QW to QD (the dependence $\tau_T(B)$ in Fig. 1c), are controlled by electron transport in the QD–QW tunneling pair.

To observe radiative transitions involving hybrid states of the *i*-TIS, we also used extremely nonequilibrium conditions caused by high-power pulsed pumping (Fig. 4b). These PL spectra show how the density of hybrid states of the QD–NB–QW system (h_{1h}; $\{h_{nh}\}$) exceeds the hole density in the QD ground and excited states (h_1; $\{h_n\}$) not subjected to hybridization.

Under electrical pumping of the *i*-TIS, electrons in the *pin* junction are injected to the e_1 level into the QD through the QW which has a large trapping cross section. Holes are injected by the *p*-GaAs buffer layer, arriving mostly at hybrid states $\{h_{nh}\}$ and h_{1h}. Thus, the overlap of electron–hole wavefunctions necessary for strengthening the NB transition is provided. Due to the existence of the drift-momentum component in the presence of nanobridges and hybrid states penetrating the entire QD–NB–QW system, hole relaxation to unfilled QD levels $\{h_n\}$ and h_1 becomes hardly probable. As a result, radiative recombination from the e_1 level occurs through hybrid hole states, and the NB band dominates in the EL spectrum in the mode of low currents (Fig. 2b).

4. CONCLUSIONS

Thus, we showed that the formation of nanobridges coupling the QD top with the QW bottom in a tunneling barrier <6 nm thick in *i*-TIS not only enhances carrier injection from QW to QD, but also leads to energy-spectrum renormalization with the result that new hybrid states and associated optical transitions appear, which are detected in the experiments and simulation. The NB radiative transition involving hybrid hole states is strengthened in the built-in electric field of the *pin* structure and(or) in the mode of low currents through the QD–NB–QW system, when it becomes a dominant EL channel. At a current density above 10 A cm^{-2}, nanobridge "burning" was detected, after which the system becomes a "quasi-classical" tunneling QD–QW pair. However, the EL efficiency of such *i*-TIS remains high and exceeds the known values for TIS with the ordinary layer sequence, which is explained by selective disabling of the QD fraction with nanobridges from the transport

processes. Currently, we are performing detailed studies of the EL modes of *i*-TIS with the aim of manipulating the ratio of the numbers of QDs with and without nanobridges. This is opening the way to single-photon emitters for the near infrared region.

ACKNOWLEDGMENTS

We are grateful to Yu. B. Samsonenko and A.I. Khrebtov for participation in the growth experiments, M. Reiche, I.P. Soshnikov, A.V. Senichev, S. Hopfer, and C. Münx for their assistance in mesa-structure fabrication, N.D. Zakharov for TEM studies, and L.V. Asryan for helpful discussions.

This study was supported by scientific programs of the Presidium of the Russian Academy of Sciences, Department of Nanotechnologies and Information Technologies of the Russian Academy of Sciences, the German Federal Ministry BMBF (grant no. 03Z2HN12), and budget grants of Saint Petersburg State University.

REFERENCES

1. L. V. Asryan and S. Luryi, Solid State Electron. **47**, 205 (2003).
2. P. Bhattacharya and S. Ghosh, Appl. Phys. Lett. **80**, 3482 (2002).
3. P. Bhattacharya, S. Ghosh, S. Pradhan, J. Singh, Z.-K. Wu, J. Urayama, K. Kim, and T. B. Norris, IEEE J. Quant. Electron. **39**, 952 (2003).
4. P. Bhattacharya and S. Fathpour, Appl. Phys. Lett. **86**, 153109 (2005).
5. V. G. Talalaev, J. W. Tomm, N. D. Zakharov, P. Werner, U. Gösele, B. V. Novikov, A. S. Sokolov, Y. B. Samsonenko, V. A. Egorov, and G. E. Cirlin, Appl. Phys. Lett. **93**, 031105 (2008).
6. V. G. Talalaev, A. V. Senichev, B. V. Novikov, J. W. Tomm, T. Elsaesser, N. D. Zakharov, P. Werner, U. Gosele, Yu. B. Samsonenko, and G. E. Cirlin, Semiconductors **44**, 1050 (2010).
7. V. G. Talalaev, A. A. Tonkikh, N. D. Zakharov, A. V. Senichev, J. W. Tomm, P. Werner, B. V. Novikov, L. V. Asryan, B. Fuhrmann, J. Schilling, H. S. Leipner, A. D. Buravlev, Yu. B. Samsonenko, A. I. Khrebtov, I. P. Soshnikov, and G. E. Cirlin, Semiconductors **46**, 1460 (2012).
8. V. G. Talalaev, A. V. Senichev, B. V. Novikov, J. W. Tomm, L. V. Asryan, N. D. Zakharov, P. Werner, A. D. Buravlev, Yu. B. Samsonenko, A. I. Khrebtov, I. P. Soshnikov, and G. E. Cirlin, Vestn. SPb. Univ., Ser. 4, No. 3, 34 (2012).
9. T. Tada, A. Yamaguchi, T. Ninomiya, H. Uchiki, T. Kobayashi, and T. Yao, J. Appl. Phys. **63**, 5491 (1988).
10. M. Nido, M. G. W. Alexander, and W. W. Ruehle, Appl. Phys. Lett. **56**, 355 (1990).
11. J. N. Zeng, I. Souma, Y. Amemiya, and Y. Oka, J. Surf. Anal. **3**, 529 (1997).
12. R. Heitz, I. Mukhametzhanov, P. Chen, and A. Madhukar, Phys. Rev. B **58**, R10151 (1998).
13. A. Tackeushi, T. Kuroda, K. Mase, Y. Nakata, and N. Yokovama, Phys. Rev. B **62**, 1568 (2000).
14. Y. I. Mazur, Z. M. Wang, G. G. Tarasov, G. J. Salamo, J. W. Tomm, and V. Talalaev, Phys. Rev. B **71**, 235313 (2005).
15. Y. Mazur, B. L. Liang, Z. M. Wang, D. Guzun, G. J. Salamo, Z. Y. Zhuchenko, and G. G. Tarasov, Appl. Phys. Lett. **98**, 083118 (2006).
16. Y. Mazur, V. G. Dorogan, E. Marega, Z. Y. Zhuchenko, M. E. Ware, M. Benamara, G. G. Tarasov, P. Vasa, C. Lienau, and G. J. Salamo, J. Appl. Phys. **108**, 074316 (2010).
17. P. N. Racec and L. I. Goray, WIAS Preprint No 1898 (2013); http://wias-berlin.de/publications/wias-publ/index.jsp?lang=1
18. A. V. Senichev, V. G. Talalaev, J. W Tomm, B. V. Novikov, P. Werner, and G. E. Cirlin, Phys. Status Solidi RRL **5**, 385 (2011).

Translated by A. Kazantsev